Chapter 3

Estimation of Cultivated Areas Using Multi-Temporal SAR Data

Nada Milisavljević, Francesco Collivignarelli and Francesco Holecz

Additional information is available at the end of the chapter

http://dx.doi.org/10.5772/58282

1. Introduction

Estimation of cultivated areas in small plot agriculture is an important issue for food security purposes in Africa. One way to obtain this information is through classical field surveys and aerial photography, which are both time and resource consuming. Multi-temporal high resolution Synthetic Aperture Radar (SAR) systems, as sources of reliable and overall information [1], [2], [3], [4], are an alternative solution, satisfying also the demand of continuous monitoring. Namely, for food security purposes, large scale agricultural products are requested at different times throughout the rain-fed crop season. Concerning the cultivated area, typically, a first product is required after the fields preparation; a second one prior to the harvesting time. In this respect, it is worth mentioning that i) the cultivated area product at start of crop season – today not available in food security services – is an excellent indicator to quantify the overall situation of the upcoming rain-fed crop season; ii) SAR systems – on the contrary to optical sensors – are suitable to map these areas due to their sensitivity to the soil roughness, a typical characteristic of the fields at this stage.

Based on these considerations, a three-step approach for estimation of cultivated area in small plot agriculture in Malawi is envisaged and presented in this chapter. The first step of this approach is the estimation of crop extent prior to the crop season. The estimation of the potential area at start of the crop season is the second step, while the third step consists in determining the crop growth extent during the rain-fed crop season. Taking into account that various vegetation types grow during the rainy season, the key issue is to know what is really cultivated and not simply vegetated. The final result is crucial when dealing with food security and agriculture in developing countries, where available land-cover map is either inaccurate,

out of date or it does not even exist. Once derived, this global information, which should give a basis for deciding where to perform more detailed analysis, should be relevant for a longer period of time in normal situations, so it should not need to be updated annually.

As shown in [5], [6], [7], [8], radar-only approaches possess an important operational advantage w.r.t. optical-only or optical-radar approaches, especially in cloud-prone regions, due to their all-weather working ability, high spatial resolution and sensitivity to biomass and moisture. In addition, the penetration depth into crop canopy depends on SAR frequency (the longer the wavelength, the longer the penetration depth) so using multi-frequency data (L-, X- and C-bands) in function of the phenological stages of crops should bring improvements in the estimation of cultivated areas [9], [10]. Finally, since the growth periods of different crops are not equal, in order to differentiate cultivated areas in small-plot agriculture from other areas with different plants and crops that are out of our interest, multi-temporal data are needed.

The main goal of the work presented here on deriving the potential crop extent prior to the start of the rain-fed season is to provide a first information layer regarding the extent of the bare soil area where crop will potentially grow. Multi-temporal L-band SAR data having resolution in the order of 15 m should be sufficient to extract this type of information. In a next step, where potential cultivated area at start of season should be looked for, a very high resolution sensor is needed. The acquisition coverage of this very high resolution sensor (such as X-band Cosmo-SkyMed with the resolution of 3 m) can be limited thanks to the output of the first step. In the final step, monitoring of the crop growth, multi-temporal ASAR (C-band, 15 m resolution) are used, starting from the period before December (in order to have the reference bare soil) as well as covering the period from December to April (the completion of crop season). Finally, several voting strategies are tested for the combination of the outputs of each of the three sensors.

The key aspect of the proposed approach is the generation of three independent and complementary products – each one with a clear meaning within agriculture and food security – derived from different spaceborne SAR sensors, which in turn are fused, by yielding the cultivated area product. Moreover, it is also intended to demonstrate the usefulness of SAR data for the targeted application. Note that in this context, the meaning of cultivated area is the effective cropped land (i.e., cultivated and not fellow land) during the rain-fed season. Commercial and irrigated fields, typically cultivated during the dry season, are out of our interest.

The chapter is organized as follows. In the following section, we briefly describe the food security situation in Malawi. Then we present the three steps of our method, one by one. For each of them, we describe the data used, the procedure, we show the obtained results and their validation using ground-truth information. After that, we present the final combination by describing our fusion methods, obtained results and their validation. Finally, we derive some conclusions.

http://dx.doi.org/10.5772/58282

2. Food security situation in Malawi

According to [11], [12], [13], [14], [15], Malawi is one of the poorest and least developed countries in Sub-Saharan Africa and a huge challenge facing Malawian agriculture is producing more food for a growing population. Many rain-fed smallholder farmers in the country have been shifting to farming systems that are increasing food crop yields and household food security. Urban poverty is increasing in Malawi as well and a pragmatic solution is seen in urban agriculture (i.e., "food production conducted in or around urban regions" [16]). Nevertheless, it is important that the amount available to small plot agriculture, especially in urban conditions, is extended with an understanding of local environmental conditions and that a careful assessment of cultivated areas in small plot agriculture is performed. As a result, the real extent of the food insecurity conditions can be estimated in order to facilitate an adequate humanitarian response if necessary and diminish the country's vulnerability to hunger.

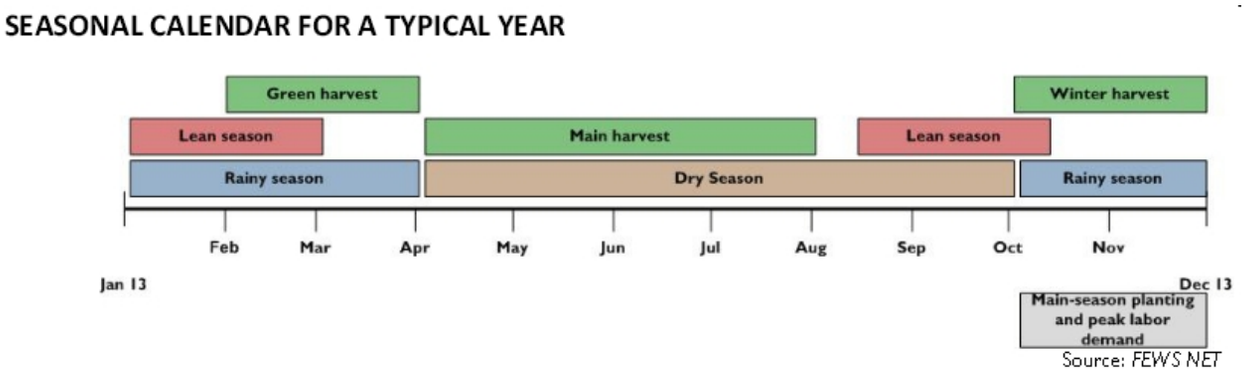

Figure 1. Seasonal calendar and critical events timeline in Malawi [17]

In Figure 1, the seasonal calendar for a typical year and critical events timeline in Malawi are shown. This country consists in three agro-ecological zones: 1) high altitude areas (more than 1300 m above sea level, cool temperatures, agricultural areas are rain-fed, with wheat and beans as main crops), 2) low altitude areas (less than 600 m above sea level, irrigated, rice, maize and beans are main crops) and 3) medium altitude areas (600-1300 m above sea level). In this chapter, the region around Lilongwe is analyzed. It belongs to medium altitude areas of Malawi that comprise about 60% of the total cultivated surface of the country. These areas are characterized by moderate temperature and a fairly long rainy season (December to February/March) and their major agriculture practice is maize. The crop calendar for maize in these areas is given in Figure 2.

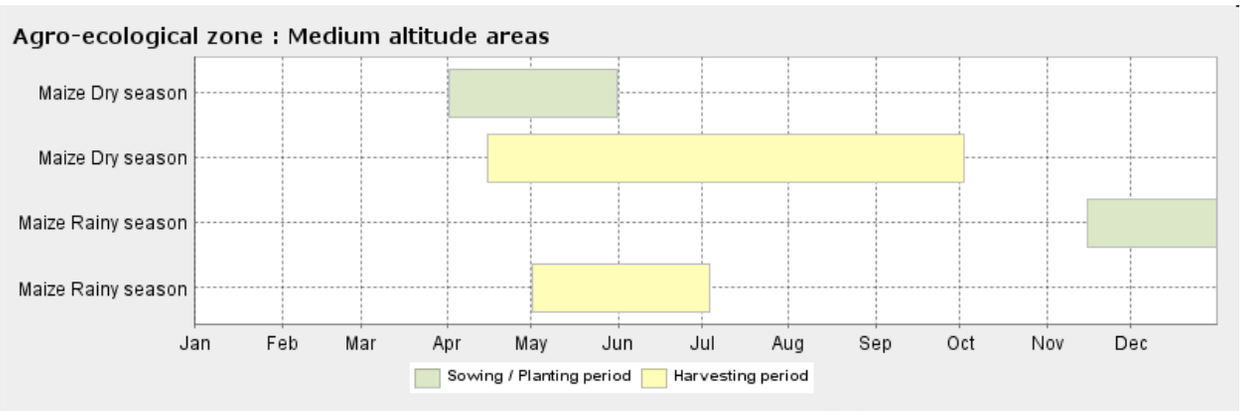

Figure 2. Generic maize crop calendar for medium altitude areas of Malawi [18]

3. First step

3.1. Multi-year L-band data

The aim of this step is to define the potential cultivable extent of the region prior to the start of the rain-fed season, in order to: 1) provide a first layer of information with the potential crop extent in bare soil conditions, i.e. the bare soil area where crop will potentially grow; 2) limit the acquisition coverage of the very high resolution sensor. The generation of this product is relevant when the available land cover map does not exist, is not updated, is inaccurate or the spatial scale is not appropriate (i.e. small scale), which are typical problems when dealing with food security and agriculture in developing countries.

Multi-temporal L-band SAR data having resolution in the order of 15 m should be sufficient to extract this type of information. Namely, in dry conditions, L-band HH/HV data have a potential of distinguishing between bare soil and other land cover classes (sparse to strong vegetation, forest, settlement, bush, wetlands, water).

Therefore, in order to estimate crop extent, multi-annual ALOS PALSAR-1 [19] acquired during the dry season are chosen, since we are interested in an average bare soil area, and not in small changes. The archive of these data, acquired by the Japanese Space Agency (JAXA), is consistent and can be processed in a multi-temporal way, which enables the speckle reduction and allows the generation of a more accurate map (based on a multi-temporal classifier) than the one obtained using a single date, because not relevant temporal variations are filtered out. Optionally, ENVISAT ASAR AP, Landsat TM-5 or SPOT-4/5 data can be used; however, in general, the latter options are not suitable, since less performing for the targeted product during the selected period. Concerning the failure of ALOS PALSAR-1 system in March 2011, it should be noticed that it does not represent a major problem, because i) the available archived data is sufficient for the generation of this intermediate product; ii) these archived data can be used even in the years to come, since the crop pattern are usually not

rapidly changing; and iii) the launch of several L-band sensors is planned in the next 1-2 years (PALSAR-2, SAOCOM-1/2).

Taking into account that the dry season prior to the start of the rainy season in Malawi is from April/May to October (Figure 2), the multi-annual PALSAR data that cover that period of the year are selected.

3.2. Procedure

As proposed in [20], preprocessed multi-temporal PALSAR data in HH and HV polarization are the input data for estimating the crop extent. The preprocessing phase consists in: multi-looking, orbital correction, co-registration, multi-temporal speckle filtering, terrain geo-coding, radiometric calibration and normalization, and anisotropic non-linear diffusion filtering. Such a preprocessing allows us to work at pixel level.

It is possible to classify these preprocessed multi-temporal SAR data using various approaches. Taking into account that our goal is to develop an approach that could be reused in other regions, where we might not have any reliable information about the existing land-cover classes, we opt for an unsupervised classification method. This means that we can either perform classification on each image separately and then combine the classification results or analyze the multi-temporal signatures of pixels or regions and perform classification based on the similarity of signatures. We choose the former in order to cover situations where we have only a few multi-temporal images or where the data are not radiometrically calibrated. The key issue at this step is to determine which pixels change in time (as a potential bare soil) and which pixels remains the same (so they can be used as a mask that covers the regions that are not interesting for further steps of our three-step method). Therefore, to each image of the multi-temporal data set, we need to apply such an unsupervised classification algorithm that preserves the grayscale information so that the classes from one image can be compared with the classes of another image and that the decision whether the class changed or not is meaningful. Based on this, our final choice is an algorithm using the Principal Components Transform (PCT) and median cut [21]. This algorithm looks for the most discriminative information based on which it divides the image into a preset number of classes, taking into account the colour (or grayscale) values.

At this step of the global approach, we have to make sure that none of the pixels that might change in time is excluded from further steps (i.e., masked as stable), while misclassifying stable pixels as changing ones is not critical here and will be further corrected in the two following steps. Due to that, we proceed in the following way. Once all the pixels of each image are classified into n classes, labeled 1, 2, …, n, they are compared and as soon as a pixel changes its label, it is marked as 0, i.e., a potential bare soil. Only if the pixel preserves its class label in all images, that is its final label too.

Taking into account that we have both HH and HV data sets, the above procedure is applied to each of the sets and the two outputs are analyzed using ground-truth information. In a final phase of the first step, these two outputs are combined and the result is compared with the

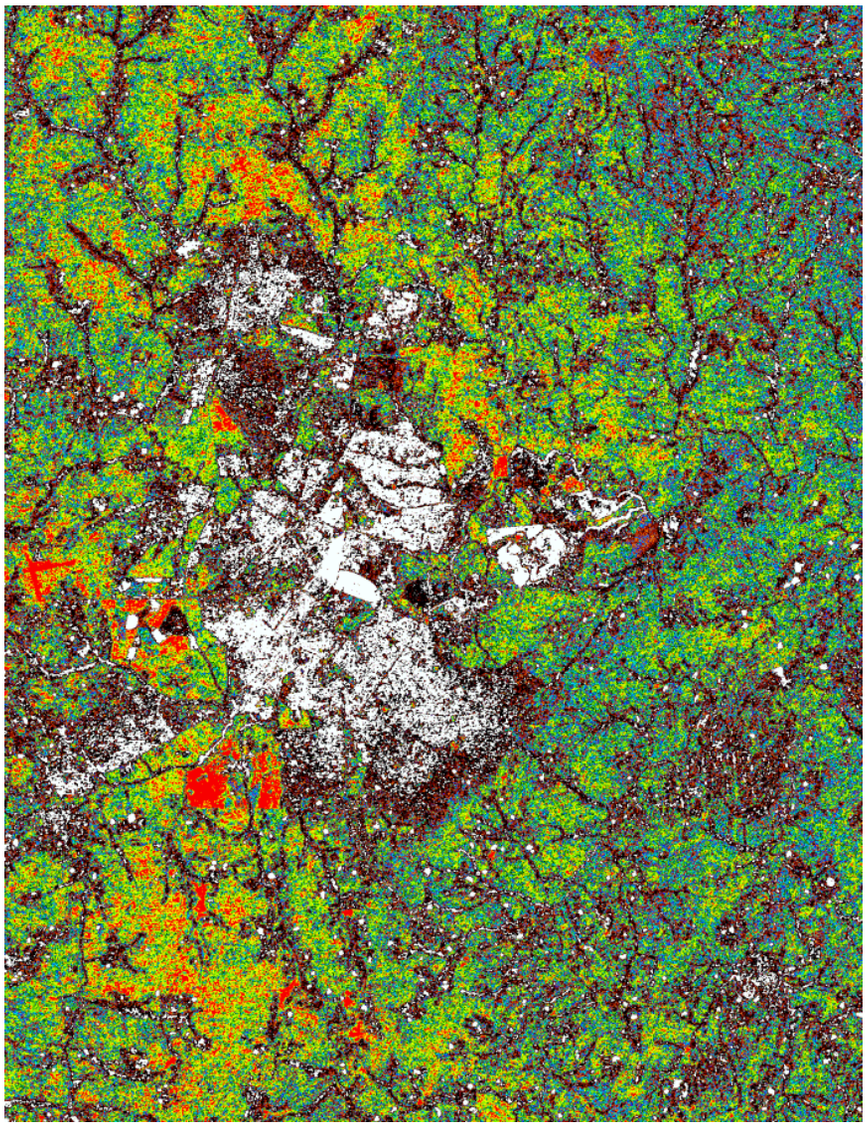

Figure 3. An example of the PALSAR HV image classification result

ground-truth as well, in order to verify the usefulness of fusing the HH/HV information at this level.

3.3. Results and validation

The test site is a relatively flat region of Malawi, around its capital, Lilongwe. We have ten ALOS PALSAR FBD (Fine Beam Double Polarisation) intensity data (so, HH and HV image pairs from ten different dates) acquired from 2007 to 2010 (from April to October each year, Figure 2). Based on the information from field, we classify each image in eight classes. (Note that we have repeated the whole procedure for ten and for twelve classes, and there was no significant change in the final result.) An example of the classified image is shown in Figure 3. The result of comparing the classification results for the HV data set is given in Figure 4, and for the HH data set, it is presented in Figure 5. Label 0 is in gray in all the images.

http://dx.doi.org/10.5772/58282

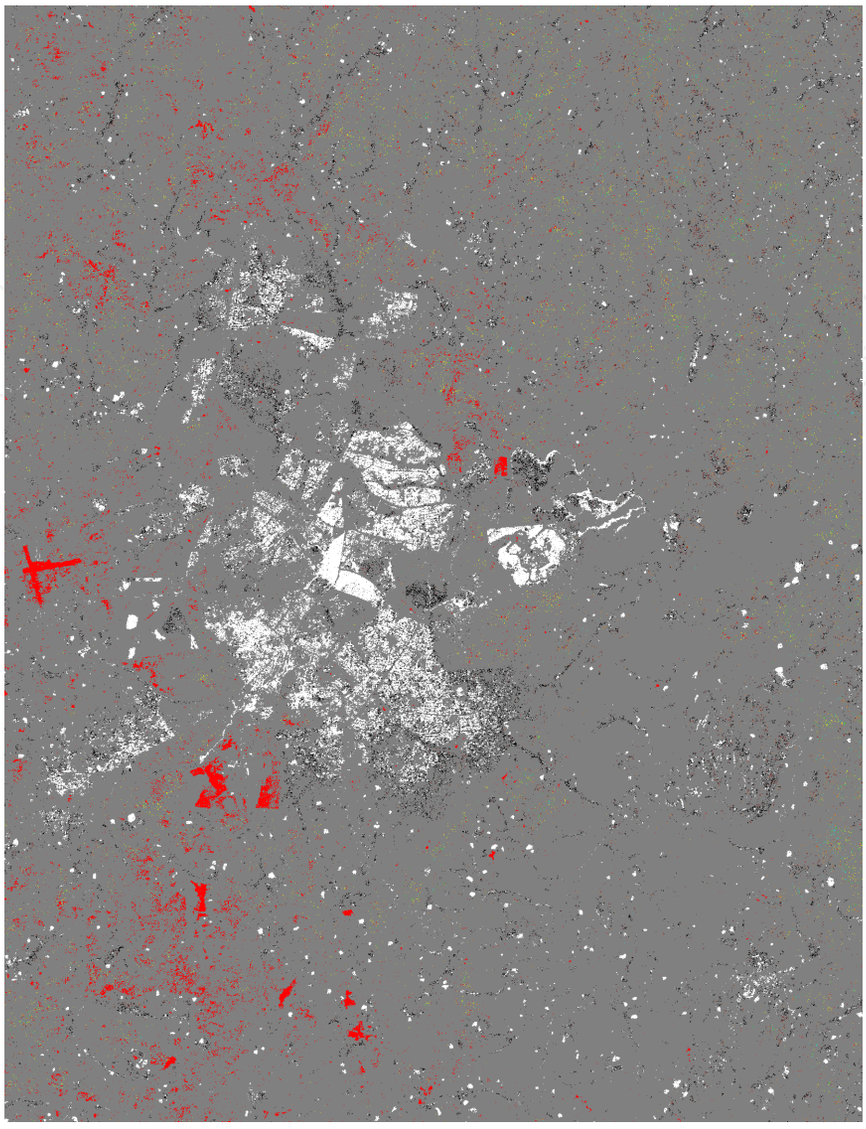

Figure 4. Comparison of the PALSAR HV classification results

Finally, a combination of the results of the HV and HH data sets is shown in Figure 6. This combination is based on the idea that if the HH and HV results label differently the pixel, its neighborhood is analyzed in HH and HV results and of the two labels, the one that is more present is chosen. If HH and HV results label equally the pixel, that label is preserved in the combined result.

As a validation, we use the ground-truth information consisting of 422 points that correspond to regions that do not change in time (buildings, water …) and 330 points that belong to arable land. For HV result (Figure 4), 202 points that do not change in time are correctly classified (having label other than 0), while 330 points that change in time are correctly labeled as 0. In the HH case (Figure 5), 91 points that belong to regions that do not change in time are well classified, and 320 points are correctly classified in case of arable land. Finally, the combination

result (Figure 6) classified well 242 points that do not change in time and all 330 points of arable land.

The final output of this step, i.e. the resulting PALSAR mask, used in further steps, is given in Figure 7. It is obtained simply by changing the color of the gray pixels from Figure 6 into white (representing potential bare soil) and assigning black colour to all other classes/colours of Figure 6 (since they are out of interest, thus masked).

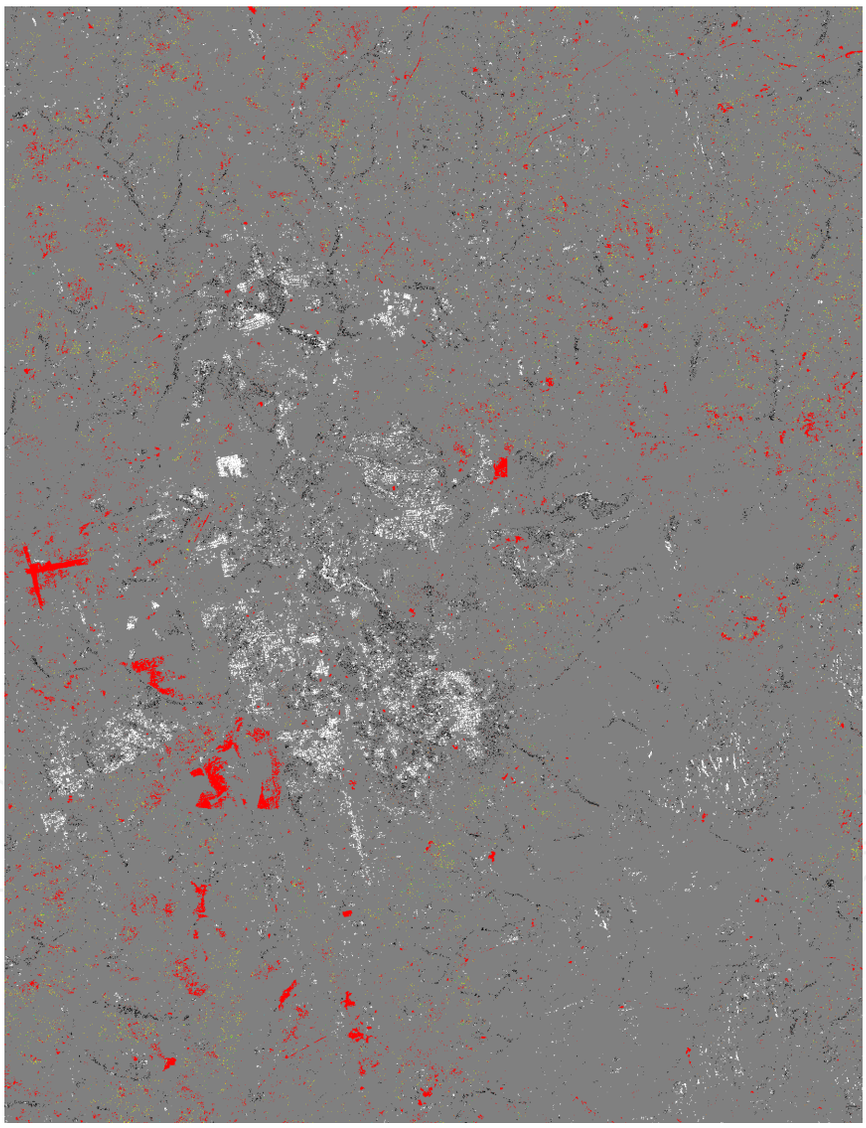

Figure 5. Comparison of the HH classification results

http://dx.doi.org/10.5772/58282

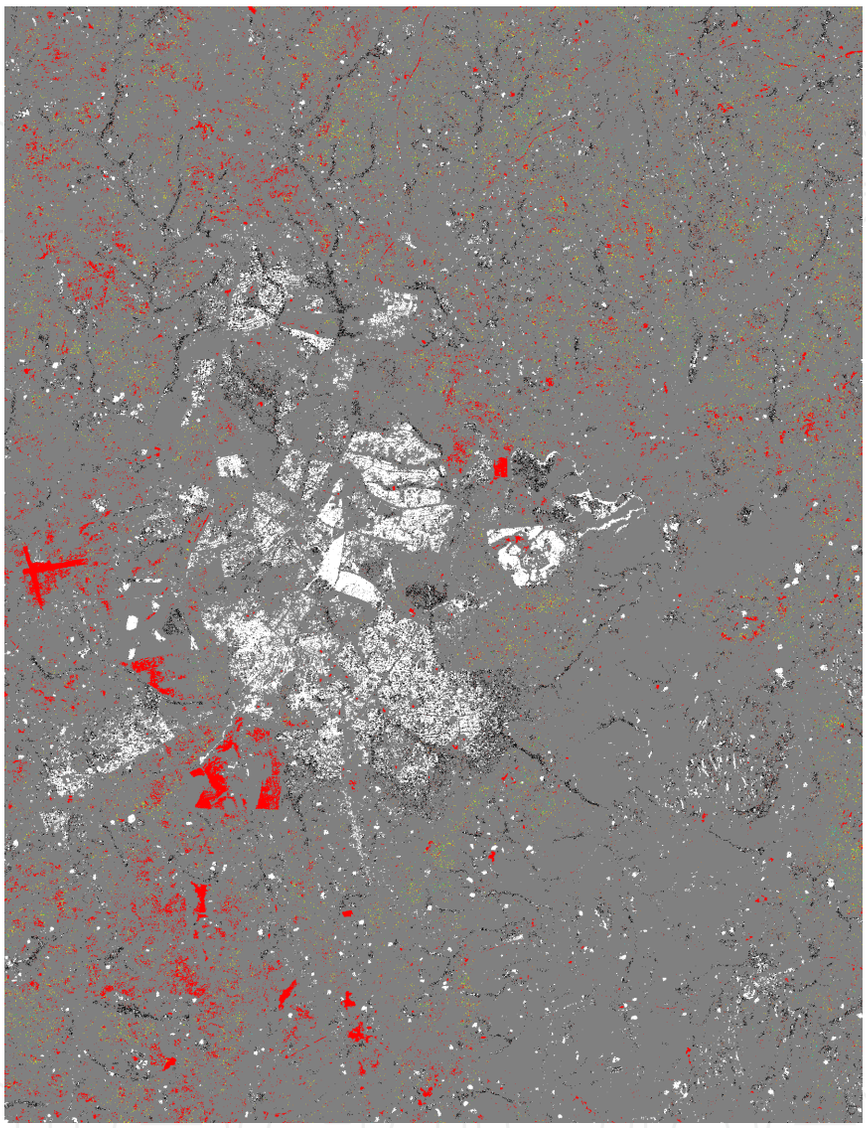

Figure 6. Combination of the HH and HV results

4. Second step

4.1. One-day interferometric X-band data

The aim of this step is to define the potential cultivated area, in particular to delineate the ensemble of fields, where crops will later grow.

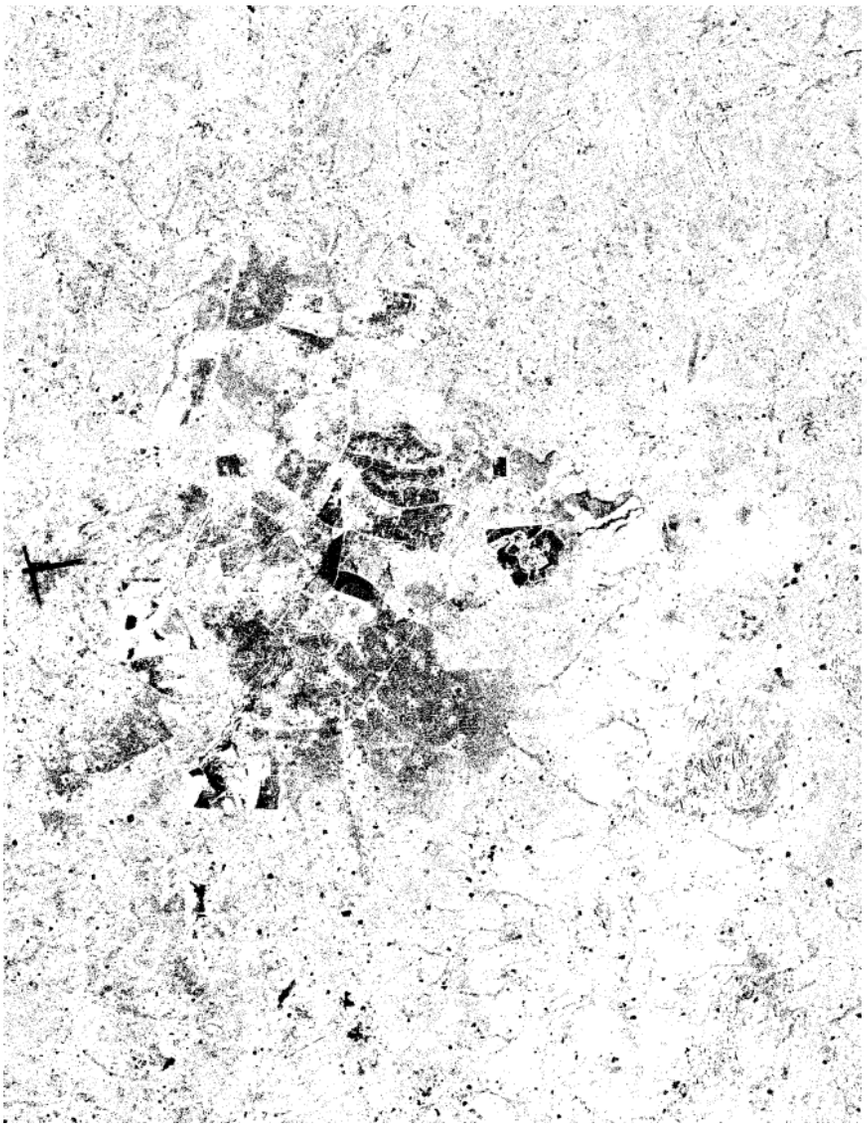

Figure 7. PALSAR mask: white – potential bare soil, black – masked.

X-band radars have the least penetration depth of the three bands used in this work, which also makes them more vulnerable to atmospheric effects. The COSMO-SkyMed (CSK) X-band SAR system is capable of acquiring data twice a day, at a high spatial resolution, which allows for very short-term analysis such as one-day correlation. Taking into account its high sensitivity and poor penetration capabilities, this system provides excellent means for analyzing short-term (lack of) changes at the very start of the crop season, when the crops are only being planted. Thus, potential cultivated area at start of season is derived from one-day interferometric CSK pair (3 m) acquired during the field preparation period.

In this respect, it is worth mentioning that this step does not have to be performed on a yearly base, if the area and the pattern of the fields remain stable: it should be exclusively updated when changes occur.

http://dx.doi.org/10.5772/58282

4.2. Procedure

Potential cultivated area at start of season is derived from one-day interferometric CSK pair acquired during the field preparation period (December, Figure 2). Very high resolution optical data would not be useful at this stage since fields are not yet covered by vegetation, so it would be very difficult to discriminate them from the surrounding bare soil area using optical sensors. On the contrary, because of the rough nature and dry conditions of the fields, short wavelength SAR data acquired in an interferometric mode (1-day interval) provide useful information at this second step.

This step should provide information on the status of the fields at the beginning of the crop season in terms of vegetated or bare soil condition. Since the purpose of the overall cultivated area product here is to map the effective crop growth from the start to the end of the crop season, only those fields with bare soil conditions are considered. This means, in terms of interferometric X-band data, that these areas are defined by a medium to high coherence (absence of human activities) and a medium to high backscattering coefficient (rough bare soil).

Image 1 Image 2	L	M	H
L	L	ML	C
M	ML	M	MH
H	C	MH	H

Table 1 Combination of two CSK amplitude images taken with one-day interval.

Taking into account that we have one one-day interferometric data set and two corresponding amplitude images, we should first combine the two amplitude images into one. Using the PCT and median cut algorithm mentioned in Subsection 3.2, we split each of the two amplitude images into three classes (L - low, M - medium and H - high amplitude). We combine them as given in Table 1, where: L – low, M – medium, H – high, C – (significant) change, ML - medium low, MH – medium high.

Amplitude Coherence	L	C	ML	M	MH	H
L	O	O	O	O	O	O
M	O	O	M1	M3	M4	H1
H	O	O	M2	M4	H1	H2

Table 2 Combination of the combined CSK amplitude image and the corresponding coherence image.

Note that the situations in which there is a strong change in the backscattering coefficient in such a short time most possibly refer to on-going works (therefore, they are most possibly not among the areas of interest).

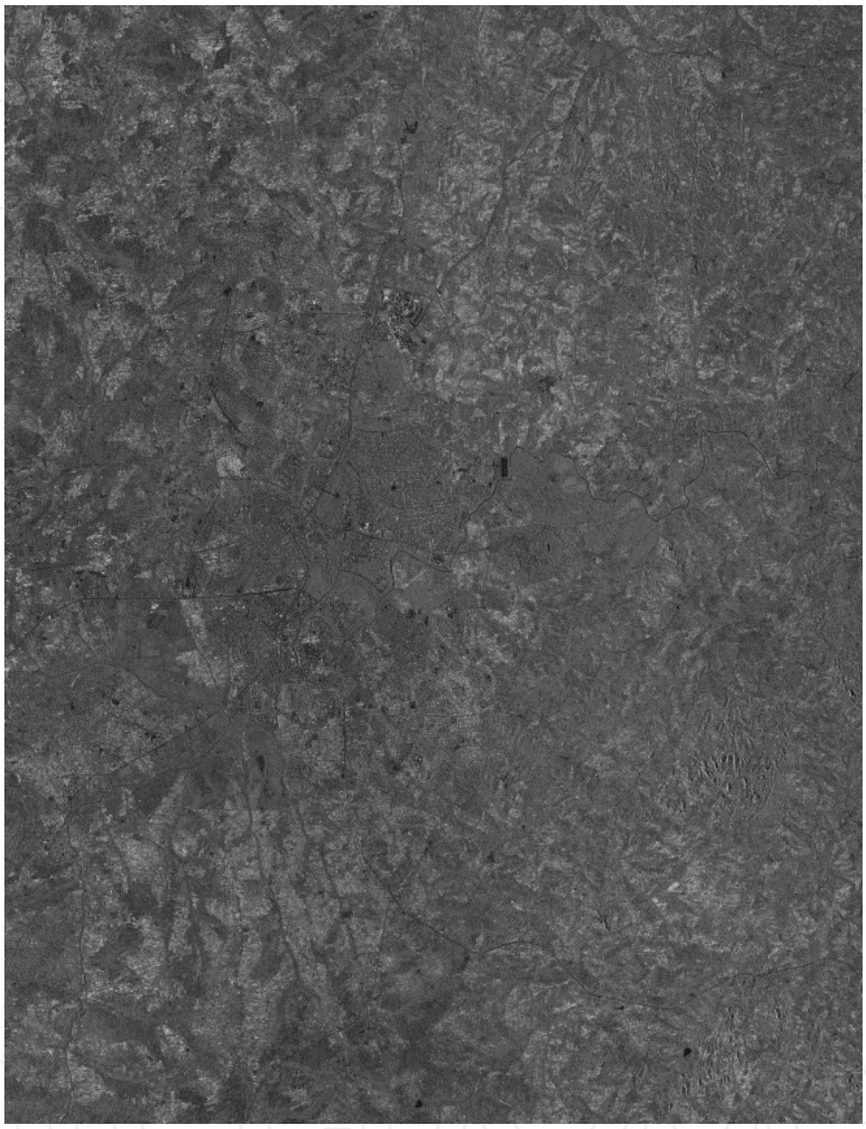

Figure 8. CSK amplitude image taken on December 9, 2010

Once the combined amplitude image is obtained, we combine this information with the corresponding coherence image, split in three classes (L, M and H) using the PCT and median cut algorithm (Subsection 3.2). The combination is based on the idea that, at this period of the year that we consider, neither low coherence nor low amplitude correspond to potential cultivated area. Thus, we combine these two data sets as indicated in Table 2, where: O – out of interest, M1 – medium 1 (one amplitude image has a low value, the other and the coherence have medium values), M2 – medium 2 (one amplitude value is low, the other is medium, coherence value is high), M3 – medium 3 (all images have medium values), M4 – medium 4

http://dx.doi.org/10.5772/58282

(two out of these three values are medium and one is high), H1 – high 1 (two out of these three values are high and one is medium), H2 – high 2 (all images have high values).

Figure 9. Result of combining the classification results of the two amplitude images from Figure 8 according to Table 1, where: L – black, C – blue, ML – green, M – yellow, MH – red, H – white.

In such a way, the order O-M1-M2-M3-M4-H1-H2 corresponds to the increasing probability that the pixel belongs to a cultivated area (bare soil).

4.3. Results and validation

Two CSK amplitude images of Lilongwe, taken on December 9 and 10, 2010 are used (the one of December 9 is shown in Figure 8, as an illustration). After splitting each of the two images in three classes (L, M and H) and combining them as indicated in Table 1, we obtain the result presented in Figure 9. Once the coherence image is split in three classes (L, M and H) and

combined with the combination of the two amplitude images following the rules of Table 2, we get the image in Figure 10.

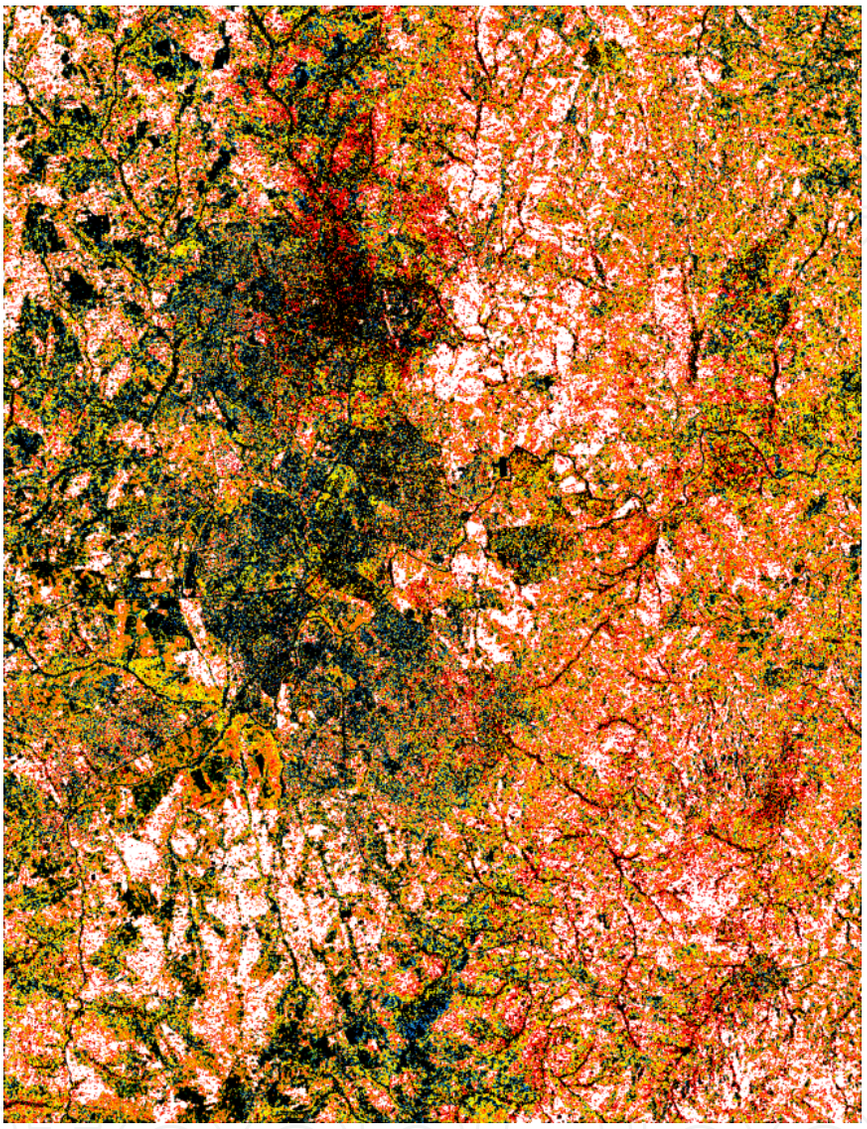

Figure 10. Result of combining the combined amplitude images from Figure 9 with the coherence image according to Table 2, where: O – black, M1 – blue, M2 – green, M3 – yellow, M4 - orange, H1 – red, H2 – white.

As far as validation is concerned, we use the same ground-truth information as described in Subsection 3.3. However, the question here is how to treat different degrees of possibility of belonging to cultivated areas, taking into account the variety of output values (O-M1-M2-M3-M4-H1-H2), i.e. where to put the threshold level between not cultivated and cultivated. If we decide to assign everything that is not O to cultivated areas, we obtain 293 (out of 330) correct classifications of bare soil and 184 (out of 422) correct classifications of the rest. If we assign O and M1 to not-cultivated areas, then we get 289 (out of 330) correct classifications of bare soil and 212 (out of 422) correct classifications for not-cultivated areas. Finally, if we assign O, M1, M2 and M3 to not-cultivated areas, we obtain

http://dx.doi.org/10.5772/58282

280 (out of 330) correct classifications of bare soil and 294 (out of 422) correct classifications for not-cultivated areas. In other words, as we move the threshold, the number of correct classifications for cultivated areas slowly decreases while the number of correct classifications for not-cultivated areas significantly increases.

Figure 11. CSK mask: white – potentially cultivated, black – masked

The final output of our approach is the combination of PALSAR (that performs very good for bare soil and moderately good for the rest, as shown in Subsection 3.3), CSK and ASAR. Thus, we should keep the threshold level for CSK in such a way that the classification of not-cultivated areas is the best possible (thus, between M3 and M4) and pay attention during the final combination so that complementarities of the three sensors are exploited in a best possible way. Figure 11 contains the image from Figure 10 where LO, M1, M2 and M3 are labeled as black (masked) and M4, H1 and H2 as white (potentially cultivated).

5. Third step

5.1. Seasonal C-band data

At this step, crop growth extent is derived from multi-temporal ENVISAT Advanced Synthetic Aperture Radar (ASAR) data [22] acquired during the crop season. Optionally, Radarsat-1/2 FB can be used at this step. Optical data such as Landsat TM-5, SPOT-4/5, Ikonos, and QuickBird, can also provide information of the crop growth. But, due to the persistent cloud coverage during this period, their use is very difficult, even more if large areas, such as national coverage, are targeted.

Multi-temporal ENVISAT ASAR (15 m) are C-band data proven to be useful in monitoring agricultural activities on a regular basis, i.e. seasonal land cover changes [1], [23], [24], [25]. Generally speaking, C-band SAR data are not hindered by atmospheric effects; their penetration capability with respect to vegetation canopies is restricted to the top layers.

5.2. Procedure

The goal of the third step is to monitor the crop growth during the crop season, which explains the necessity of having multi-temporal data acquired regularly all along the crop season. In such a way, the confusion between cropped and the surrounding vegetated, non-crop, areas should be reduced, and at the same time, the crop development could be monitored.

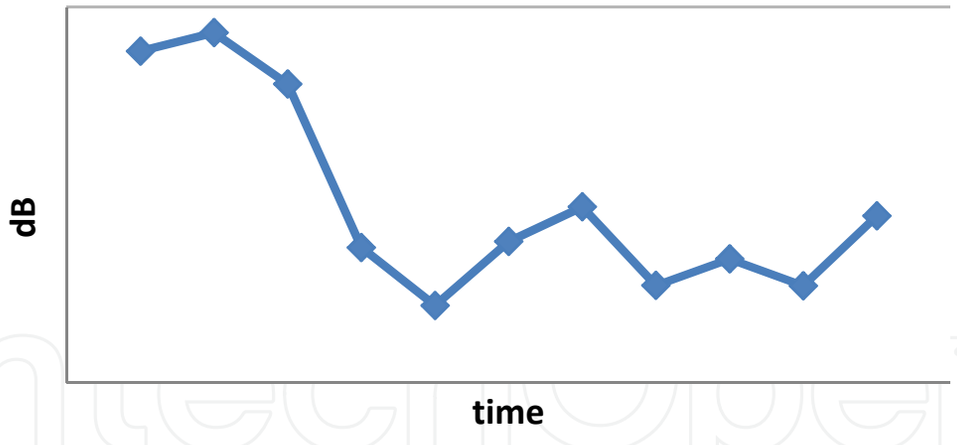

Figure 12. An illustration of the typical behavior of the C-band maize signature (intensity in function of time) from the beginning to the end of the season.

Our procedure for analyzing the ASAR data is as follows. Firstly, we perform an unsupervised classification based on multi-temporal signatures (so, grouping together the pixels having a similar multi-temporal behavior) in a preset number of classes. As a result, we have an output image where the pixels with similar signature have the same label. As this is an unsupervised classification, we are unable to determine which of these signatures is similar to the one of maize. Thus, in the following level of our analysis, we introduce our knowledge regarding the maize signature at C-band (note that, depending on the area, season and the type of the crop

http://dx.doi.org/10.5772/58282

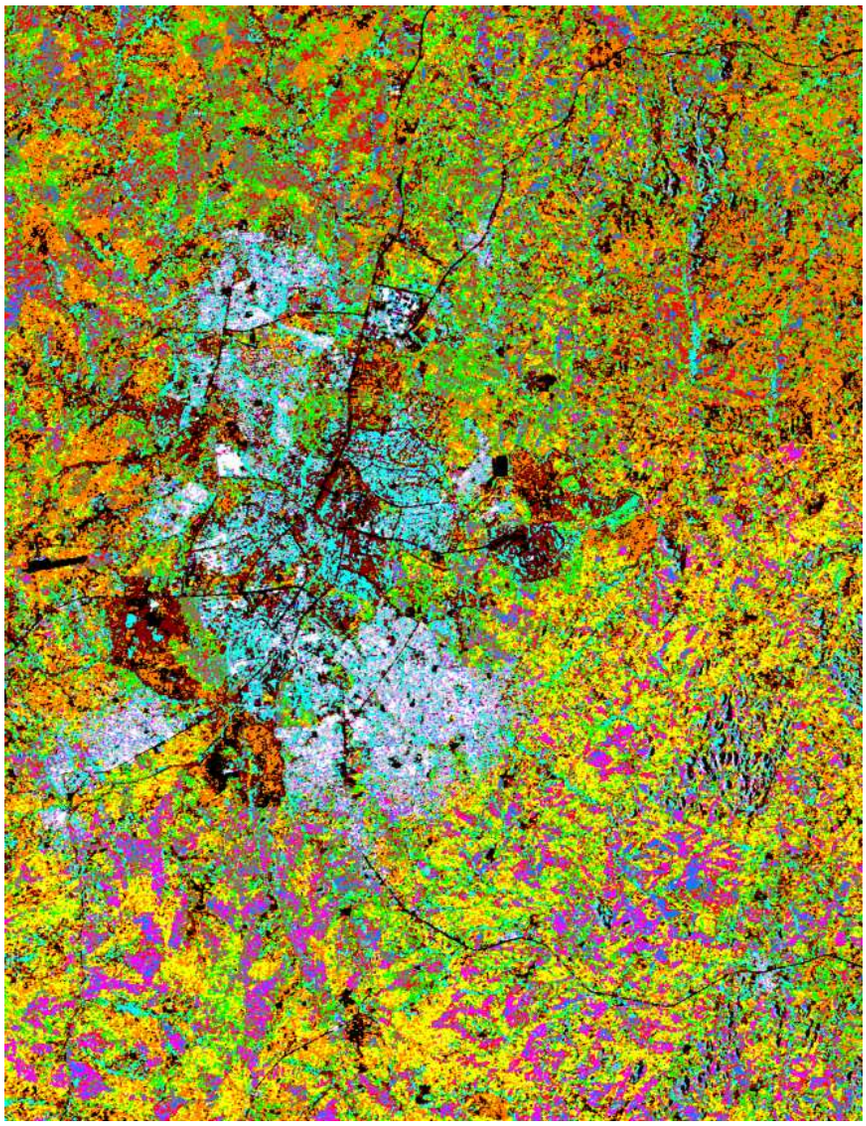

Figure 13. Result of an unsupervised classification based on multi-temporal pixel behavior in eleven ASAR images

we want to distinguish, this step can be easily modified for other applications): at the very beginning of the season, the intensity of the signature is low, and then it grows, reaching rapidly its maximum value (which corresponds to ploughing), and then dropping to its first minimum (sowing). Then the second phase begins, i.e. from flowering to plant drying stage, where the intensity of the signature raises, reaches another maximum, possibly drops a bit and raises again, in function of the plant moisture and the surface scattering at the top of the plant. This behavior is similar to the one illustrated in Figure 12. Since the later stages can vary from season to season, the key indicators we use to select which of the signatures from the unsupervised classification output resemble to the one of maize are the starting raise of the signature, its sudden drop followed by its next raise. Thus, we analyze the moments when the first maximum, the first minimum and the second maximum occur and label the class(es) with the corresponding tendencies as the one(s) of maize.

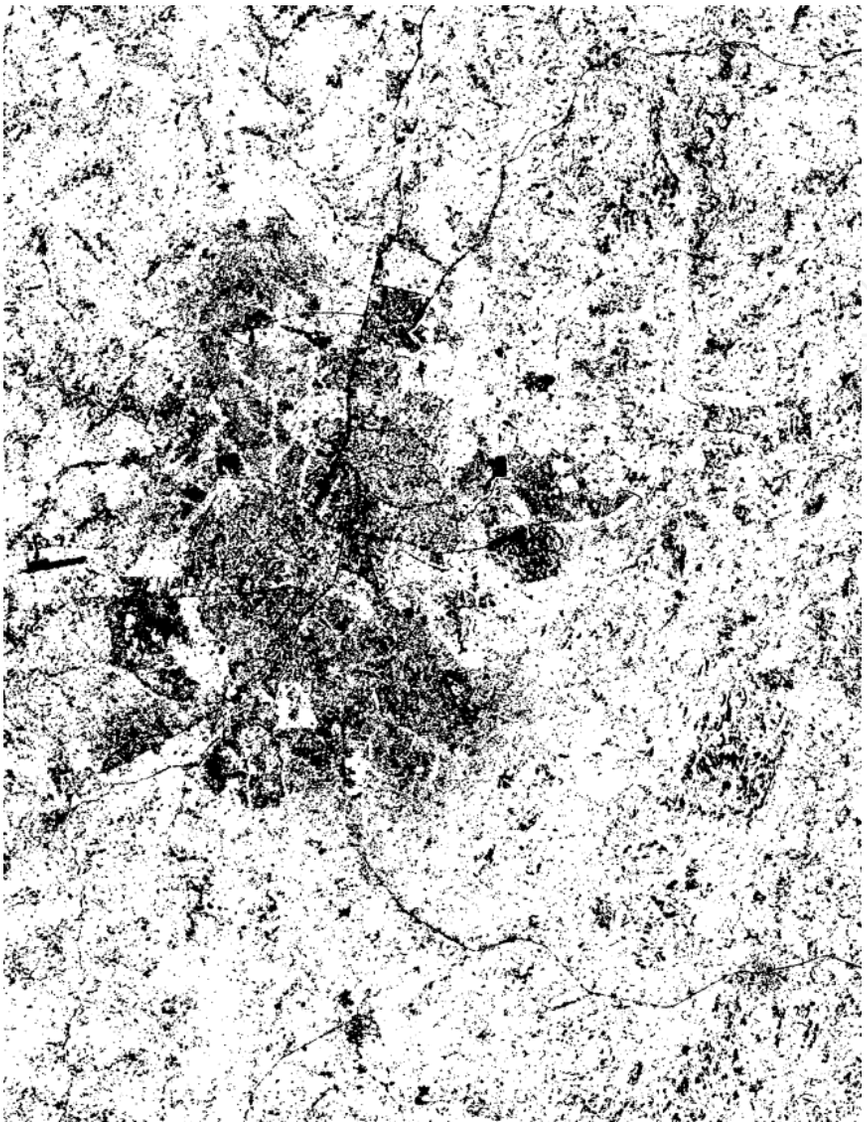

Figure 14. Grouping of the classes from Figure 13: white – crop growing extent, black – the rest (masked)

5.3. Results and validation

Once a multi-temporal unsupervised classification of multi-temporal pixel signatures in twelve classes is performed, using eleven ASAR intensity images covering the period from September 2010 to March 2011, we obtain the result given in Figure 13. After analyzing the multi-temporal signatures of each of twelve classes, we select the classes having tendencies similar to the ones of maize (Figure 12), and we mask the rest. The obtained result is given in Figure 14. Note that the classification has been also performed in eight and ten classes and that there was no significant change in the final result.

The validation results are as follows: 303 (out of 330) pixels from cultivated areas are well classified, as well as 235 (out of 422) pixels from non-cultivated areas.

http://dx.doi.org/10.5772/58282

6. Final combination

6.1. Procedure

There are various methods of combining the results obtained from each of the three sensors, depending on the quality of each of the sensors, requested computation speed, application, etc. In our case, looking for a simple, fast yet reliable method, we test several voting combination rules:

- ANDc (a pixel is declared as cultivated if all sensors labeled it as such; it is masked otherwise);
- ANDm (for the masked class: a pixel is declared as masked if all sensors labeled it as such; otherwise, it is declared as potentially cultivated);
- MAJ (for class labeled as potentially cultivated: if at least two out of three sensors labeled it as potentially cultivated, the pixel is labeled at the combination output as cultivated; otherwise, it is masked), and
- OR (for class labeled as potentially cultivated: a pixel is declared as masked only if all sensors labeled it as such; otherwise, i.e., if at least one of the sensors labeled a pixel as potentially cultivated, it will keep that label at the combination output).

Note that the difference between ANDc and ANDm is that in the former case, AND voting is applied to the cultivated class while in the latter case, AND voting is applied to the masked class. This makes the two AND voting approaches complementary and it depends on the application which one is more useful than the other. Finally, the difference between MAJ and OR is that the former labels a pixel as potentially cultivated if at least two of the three sensors have given it that label and it is masked otherwise, while the latter labels a pixel as potentially cultivated if any of the three sensors labeled it as such.

6.2. Results and validation

The four voting strategies are applied to the outputs of the three sensors given in Figures 7, 11 and 14. As an illustration, Figure 15 contains the result of ANDc voting, while the result of MAJ voting is shown in Figure 16.

We validate these results using the same validation set as in the previous steps and obtain the following results:

- ANDc voting: 225 out of 330 pixels from cultivated fields well classified; 377 out of 422 pixels belonging to non-cultivated fields well classified;
- ANDm voting: all 330 pixels belonging to cultivated fields well classified, as well as 78 out of 422 pixels from non-cultivated fields;
- MAJ voting: all 330 pixels from cultivated fields well classified, as well as 323 out of 422 pixels from non-cultivated fields;

- OR voting: all 330 pixels from cultivated fields well classified, as well as 59 out of 422 non-cultivated field pixels.

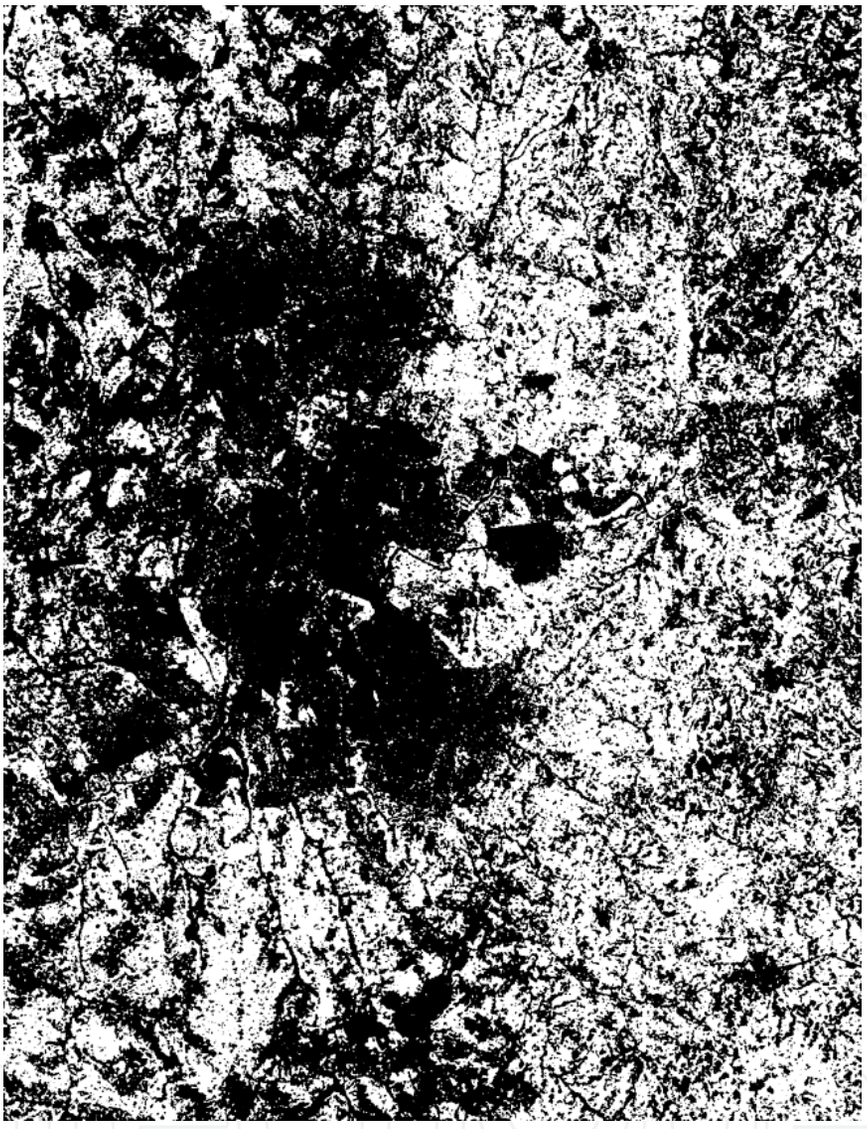

Figure 15. Result of ANDc voting: white – crop growing extent, black – masked.

These validation results are in accordance with our expectations. Namely, if we keep as cultivated only those pixels where all three sensors claim that it is cultivated indeed, and label all the rest as masked (non-cultivated), we can expect to have a high detection of non-cultivated fields and only modest results for cultivated fields (ANDc voting). With the inverse logic, we preserve all cultivated fields, but also label many non-cultivated as being cultivated (ANDm voting, as well as OR). Finally, with the majority voting (MAJ), it can be expected to obtain results that optimize the two extremes, and benefit from the complementarities of the sensors.

http://dx.doi.org/10.5772/58282

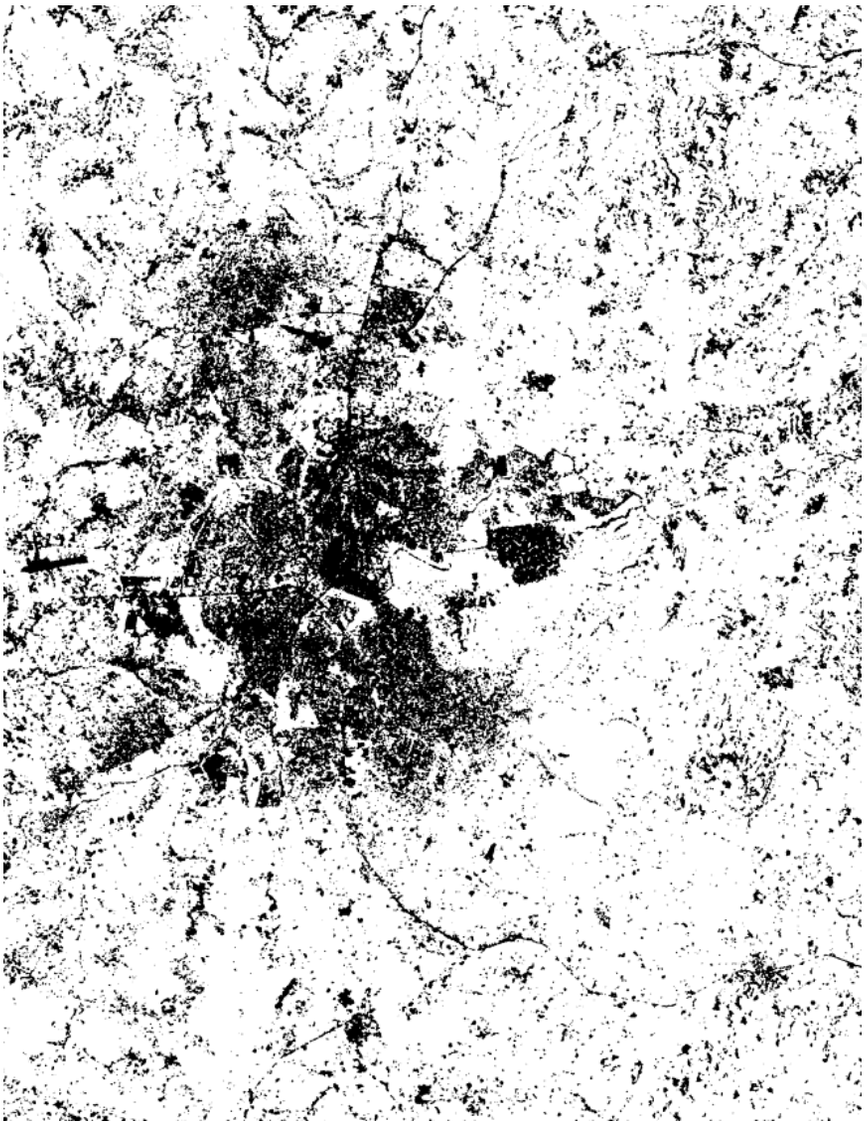

Figure 16. Result of MAJ voting: white – crop growing extent, black – masked.

The same conclusion can be derived from Table 3, which represents the summary of the validation results, for each of the steps and each of the combination approaches tested. From the three steps, step 1 has the best correct classification of pixels belonging to cultivated fields, but 42.64% of pixels belonging to non-cultivated fields are also classified as cultivated. On the other hand, step 2 has the best correct classification of pixels from non-cultivated fields, but 15.15% of cultivated field pixels are also classified as non-cultivated. Regarding the four fusion strategies used, we can conclude that with the MAJ voting, we preserve the maximum number of correct classifications as the one of PALSAR in step 1, while we increase the correct classification of non-cultivated fields as well, thanks to the output of CSK and ASAR. Although the priority is not to miss cultivated fields, an improvement in correct classification of non-cultivated fields is also an important issue since it leads to a better estimation of the extent of the problem.

	cultivated fields well classified (out of 330)	non-cropped fields well classified (out of 422)
step 1	100%	57.35%
step 2	84.85%	69.67%
step 3	91.82%	55.69%
final ANDc	68.18%	89.34%
final ANDm	100%	18.48%
final MAJ	100%	76.54%
final OR	100%	13.98%

Table 3 Correct classifications: summary of the validation results (in percents)

Note that the validation is performed on the pixel level. If done on the region level, the validation results would certainly have been even better since a region would have been declared as correctly classified if majority of its pixels (and not all of them, as here) were correctly classified.

The achieved accuracy confirms the validity of the methodology, in particular that: 1) the use of very high resolution data is an indispensable condition for the identification of small agricultural plots; 2) the differentiation between cultivated areas (i.e. growing vegetation during the crop season) and other land cover classes is first and foremost possible if multi-temporal data are used; 3) the combination of various SAR sensors (bands) improves the final results.

7. Conclusion

Agriculture is the land cover type showing the largest spatial and temporal dynamics during a relatively short period. Therefore, pre-requisite for the generation of an accurate cultivated area product is to combine very high resolution data with multi-temporal high resolution data acquired throughout the whole crop season. This approach has been tested through a three-step procedure for estimation of cultivated area in small plot agriculture in Malawi and the obtained results have proven its validity.

The first step of this procedure is the estimation of crop extent prior to the crop season using multi-temporal L-band PALSAR data. The estimation of the potential area at start of the crop season using X-band COSMO-SkyMed is the second step, while the third step consists in determining the crop growth extent during the rain-fed crop season, with the help of multi-temporal C-band ASAR data. The final result is crucial when dealing with food security and agriculture in developing countries, where available land-cover map is either inaccurate, out of date or it does not even exist. Once derived, this global information, which should give a

http://dx.doi.org/10.5772/58282

basis for deciding where to perform more detailed analysis, should be relevant for a longer period of time in normal situations, so it should not need to be updated annually.

At each step, the obtained results are validated using ground-truth information.

Four voting combination strategies are tested in the final combination of the three sensors, based on "majority", "or" and "and" logic (two versions of it - one prioritizing cultivated, and the other non-cultivated fields). For our application, the majority voting gives the most interesting results of the four, while for some other applications (such as mined area reduction, for example), one of the other strategies might be useful.

As demonstrated here, the spatial resolution of existing space-borne remote sensing systems and the wise integration of different remote sensing sources enable the achievement of a high level of detail and accuracy, as long as the data are understood, processed and used in the right way. The proposed solution is attractive, less time consuming and less expensive compared to area regression estimators exclusively based on field survey. Furthermore, the remote sensing solution intrinsically provides a monitoring component (as agricultural area can vary during a season): this is often (or fully) not taken into account in the area regression estimator approach, simply because it is too time consuming to frequently repeat the field survey.

In our future work, other combination approaches will be tested, in order to optimize the exploitation of the complementarities of the three SAR sensors.

Acknowledgements

The European, Japanese, and Italian Space Agency are acknowledged for the provision of the ENVISAT ASAR, ALOS PALSAR-1, and Cosmo-SkyMed data. EFTAS, C-ITA, and the Ministry of Agriculture and Food Security of Malawi are acknowledged for the collection and provision of the ground survey data in Malawi.

This work has been done in the scope of the SARLAT project launched by the Belgian Ministry of Defense.

Author details

Nada Milisavljević[1], Francesco Collivignarelli[2] and Francesco Holecz[2]

1 Department of Communication, Information Systems & Sensors (CISS), Royal Military Academy, Brussels, Belgium

2 Sarmap, Purasca, Switzerland

References

[1] F. Holecz, M. Barbieri, A. Cantone, P. Pasquali and S. Monaco, "Synergetic Use of Multi-temporal ALOS PALSAR and ENVISAT ASAR Data for Topographic/land Cover Mapping and Monitoring at National Scale in Africa," in *IEEE International Geoscience & Remote Sensing Symposium (IGARSS 2009)*, Cape Town, South Africa, 2009.

[2] V. Krylov and J. Zerubia, "High resolution SAR image classification," Technical report 7108, INRIA Sophia Antipolis, France, 2009.

[3] N.-W. Park, "Accounting for temporal contextual information in land-cover classification with multi-sensor SAR data," *International Journal of Remote Sensing 31(2),* pp. 281-298, 2010.

[4] D. Bargiel and S. Herrmann, "Multi-Temporal Land-Cover Classification of Agricultural Areas in Two European Regions with High Resolution Spotlight TerraSAR-X Data," *Remote Sensing 3(5),* pp. 859-877, 2011.

[5] H. McNairn, J. Ellis, J. J. van der Sanden, T. Hirose and R. J. Brown, "Providing crop information using RADARSAT-1 and satellite optical imagery," *International Journal of Remote Sensing 23(5),* pp. 851-870, 2002.

[6] X. Blaes, L. Vanhalle and P. Defourny, "Efficiency of crop identification based on optical and SAR image time series," *Remote Sensing of Environment 96(3),* pp. 352-365, 2005.

[7] J. Shang, H. McNairn, C. Champagne and X. Jiao, "Application of Multi-Frequency Synthetic Aperture Radar (SAR) in Crop Classification," in *Advances in Geoscience and Remote Sensing*, InTech, DOI: 10.5772/8321, 2009.

[8] X. Wang, L. Ge and X. Li, "Pasture Monitoring Using SAR with COSMO-SkyMed, ENVISAT ASAR, and ALOS PALSAR in Otway, Australia," *Remote Sensing 5,* pp. 3611-3636, 2013.

[9] X. Jiao, H. McNairn, J. Shang and J. Liu, "The Sensitivity of Multi-Frequency (X, C and L-Band) Radar Backscatter Signatures to Bio-Physical Variables (LAI) over Corn and Soybean Fields," in *ISPRS TC VII Symposium—100 Years ISPRS*, Vienna, Austria, 2010.

[10] R. Fieuzal, F. Baup and C. Marais-Sicre, "Sensitivity of TerraSAR-X, RADARSAT-2 and ALOS satellite radar data to crop variables," in *IEEE International Geoscience and Remote Sensing Symposium (IGARSS 2012)*, Munich, Germany, 2012.

[11] D. P. Garrity, F. K. Akinnifesi, O. C. Ajayi, S. G. Weldesemayat, J. G. Mowo, A. Kalinganire, M. Larwanou and J. Bayala, "Evergreen Agriculture: a robust approach to sustainable food security in Africa," *Food Security 2(3),* pp. 197-214, 2010.

[12] D. D. Mkwambisi, E. D. G. Fraser and A. J. Dougill, "Urban Agriculture and Poverty Reduction: Evaluating how Food Production in Cities Contributes to Food Security,

Employment and Income in Malawi," *Journal of International Development 23(2),* pp. 181-203, 2011.

[13] M. Douillet, "La relance de la production agricole au Malawi: succès et limites," Fondation pour l'agriculture et la ruralité dans le monde (FARM), Montrouge, France, 2012.

[14] F. Ellis and E. Manda, "Seasonal Food Crises and Policy Responses: A Narrative Account of Three Food Security Crises in Malawi," *World Development 40(7),* p. 1407–1417, 2012.

[15] M. Tafirenyika, "What went wrong? Lessons from Malawi's food crisis," *Africa Renewal 26(3),* p. 9, 2013.

[16] L. J. A. Mougeot, "Urban agriculture: Definition, presence, potential and risks," in *Growing Cities, Growing Food: Urban Agriculture on the Policy Agenda, a Reader on Urban Agriculture*, Feldafing, Germany, German Foundation for International Development (DSE), 2000, pp. 1-42.

[17] FEWSNet, "Malawi Food Security Outlook," July 2013. [Online]. Available: http://www.fews.net/docs/Publications/Malawi_OL_07_2013.pdf. [Accessed 17 September 2013].

[18] Food and Agriculture Organization of the United Nations (FAO), "Crop calendar" [Online]. Available: http://www.fao.org/agriculture/seed/cropcalendar/searchbycountry.do. [Accessed 24 11 2013].

[19] A. Rosenqvist, M. Shimada and M. Watanabe, "ALOS PALSAR: Technical outline and mission concepts," in *Proceedings of 4th International Symposium on Retrieval of Bio- and Geopyhisical Parameters from SAR Data for Land Applications*, Innsbruck, Austria, 2004.

[20] N. Milisavljević, F. Holecz, I. Bloch, D. Closson and F. Collivignarelli, "Estimation of crop extent using multi-temporal PALSAR data," in *IEEE International Geoscience and Remote Sensing Symposium (IGARSS 2012)*, Munich, Germany, 2012.

[21] S. E. Umbaugh, Digital Image Processing and Analysis: Human and Computer Vision Applications with CVIPtools, Boca Raton, USA: CRC Press, Taylor & Francis Group, 2011.

[22] Y. L. Desnos, C. Buck, J. Guijarro, J.-L. Suchail, R. Torres and E. Attema, "ASAR – Envisat's Advanced Synthetic Aperture Radar," *ESA Bulletin, No. 102,* pp. 91-100, May 2000.

[23] S. M. Tavakkoli, P. Lohmann and U. Soergel, "Multi-temporal Segment-based Classification of ASAR Images of an Agricultural Area," in *Global Change Issues in Developing and Emerging Countries: Proceedings of the 2nd Göttingen GIS and Remote Sensing Days 2006*, Göttingen, Germany, Universitätsverlag Göttingen, 2007, pp. 175-188.

[24] S. M. Tavakkoli Sabour, P. Lohmann and U. Soergel, "Monitoring Agricultural Activities using Multi-temporal ASAR ENVISAT Data," in *Proceedings of XXIst ISPRS Congress "Silk Road for Information from Imagery", Vol.XXXVII, ISSN 1682-1750*, Beijing, China, 2008.

[25] A. Bouvet and T. L. Toan, "Use of ENVISAT/ASAR wide-swath data for timely rice fields mapping in the Mekong River Delta," *Remote Sensing of Environment 115(4)*, pp. 1090-1101, 2011.

IntechOpen